Monthly Notices
of the
ROYAL ASTRONOMICAL SOCIETY

MNRAS **431,** 2645–2654 (2013)
Advance Access publication 2013 March 21

doi:10.1093/mnras/stt359

Model on pulsed GeV radiation from magnetars

J. Takata,⋆ Y. Wang, E. M. H. Wu and K. S. Cheng

Department of Physics, University of Hong Kong, Pokfulam Road, Hong Kong

Accepted 2013 February 23. Received 2013 February 20; in original form 2012 July 12

ABSTRACT

We discuss a possible scenario for radiation mechanism of pulsed GeV γ-rays from magnetars. The magnetars have shown frequent X-ray bursts, which would be triggered by crust fractures and could release the energy of order of $E_{\rm tot} \sim 10^{41-42}$ erg. If the location of the crust cracking of the magnetic field is close to the magnetic pole, part of the released energy may excite the Alfvén wave that can propagate into outer magnetosphere. The oscillation of the magnetic field induces the available potential drop $\delta\Phi_{\rm p} \sim 10^{15}$ V, which can accelerate the electrons and/or positrons to the Lorentz factor $\Gamma \sim 10^7$ in the outer magnetosphere. The curvature radiation process at outer magnetosphere can produce GeV γ-rays. If the radiation process is occurred above $r \sim 5 \times 10^7$ cm from the stellar surface, the emitted GeV γ-rays can escape from the pair-creation process with the X-rays and/or the magnetic field. The expected luminosity of the GeV emissions is order of $L_\gamma \leq 10^{35}$ erg s^{-1}, and the radiation process will last for a temporal scale of years. The expected pulse profiles have a broad shape with sometimes sharp peaks. We apply the model to anomalous X-ray pulsar 1E 2259+586.

Key words: radiation mechanisms: non-thermal – waves – stars: magnetars stars: magnetic field – gamma-rays: stars.

1 INTRODUCTION

Soft γ-ray repeaters (SGRs) and anomalous X-ray pulsars (AXPs) have been discussed in terms of 'magnetar' model, in which the activities of the neutron star are powered by the dissipation of the extremely strong magnetic field (Thompson & Duncan 1995; Thompson, Lyutikov & Kulkarni 2002; Woods & Thompson 2006; Mereghetti 2008). The magnetar's emissions mainly appear in the X-ray bands, which are described by the blackbody component (with hard tail) below 10 keV plus a hard power-law component above 10 keV (Kuiper et al. 2006). The power-law components are often explained by the resonant Compton scattering process of the mildly relativistic electrons and/or positrons below 10 keV (Fernández & Thompson 2007; Rea et al. 2008) and of the relativistic pairs above 10 keV (Baring & Harding 2007; Beloborodov & Thompson 2007; Beloborodov 2013), respectively.

Although no pulsed GeV emissions from the magnetars have been confirmed, it has not been conclusive that the magnetars are intrinsically dark in the GeV radiation or present sensitivity of the *Fermi* telescope is not enough to detect any pulsed GeV emission from magnetars. It has been argued that the rotation powered activities of the magnetars can produce the γ-rays from e.g. the outer gap accelerator (Cheng & Zhang 2001). However, because temperature of the surface X-ray emissions of the magnetars is $kT \sim 0.5$ keV, which is much higher than the typical surface temperature $kT \sim 0.1$ keV of the young pulsars, the size of the outer gap, and resultant power of the γ-ray emissions will be relatively smaller than those of the canonical γ-ray pulsars, indicating less possibility for the detection of the pulsed γ-ray emissions from the outer gap of the magnetar.

Recently, GeV γ-rays from the supernova remnant (SNR) CTB 109, which will be associated with AXP 1E 2259+586, have been found in data of *Fermi* γ-ray telescope (Castro et al. 2012). Although the emissions from SNR CTB 109 has been suggested (Castro et al. 2012), the origin has not been confirmed yet. Because the future *Fermi* observations will allow us a more deep search of the GeV emissions from the magnetars, it will be worth to discuss the possible mechanism of GeV γ-ray emissions in the magnetosphere of the magnetar.

The magnetar's X-ray/γ-ray radiations powered by the magnetic energy have been discussed with the emission process near the stellar surface $r < 10^7$ cm (e.g. Beloborodov 2013). In such a case, the GeV γ-rays cannot escape from the pair-creation processes with the X-rays and/or the magnetic field, as we will discuss in Section 2. In this paper, therefore, we will discuss a possible scenario for the GeV emissions process powered by the magnetic energy in the outer magnetosphere. In Section 2, we will discuss the pair-creation processes of the GeV γ-rays and critical radial distance above which the produced GeV γ-rays can escape from the pair-creation processes. In Section 3, we will argue that Alfvén wave will be excited by crust cracking of the magnetic field and carries the released energy into outer magnetosphere along the background magnetic field line. We will discuss the possible acceleration mechanism due to the propagation of the Alfvén wave in the outer magnetosphere. We will also estimate the Lorentz factor of the accelerated particles and

⋆ E-mail: takata@hku.hk

the typical energy of the curvature radiation process. We will calculate the expected pulse profiles in Section 3.4 and γ-ray spectra in Section 3.5. In Section 4, after brief summary of the results, we will discuss the possibility of the detection for the pulsed GeV radiation from the magnetars.

2 PAIR-CREATION PROCESSES AND GEV γ-RAY EMISSION REGION

The ultrastrong surface magnetic field of the magnetars permits one-photon pair-creation process, $\gamma + B \rightarrow e^+ + e^-$ (Harding & Lai 2006). The condition of the magnetic pair-creation process occurred at a radial distance r from the neutron star may be written down as (Ruderman & Sutherland 1975)

$$\frac{E_\gamma}{2m_e c^2}\frac{B_{\rm d}(r)\sin\theta_{kB}}{B_{\rm c}} \geq \chi \quad \text{for } B_{\rm d}(r)/B_{\rm c} < 0.1, \tag{1}$$

where $\chi \sim 0.1$, E_γ is photon's energy, $B_{\rm d}(r)$ is the global dipole magnetic field at r and $B_{\rm c} = 4.4 \times 10^{13}$ G is the critical magnetic field strength. In addition, $m_e c^2$ is the electron rest mass energy and θ_{kB} is the angle between the magnetic field and the propagation direction of the photon. Using the dipole magnetic field, we estimate the radial distance, above which GeV γ-rays can escape from the magnetic pair-creation process,

$$r_{\rm m} = 3\times10^7 \left(\frac{\chi}{0.1}\right)^{-1/3}\left(\frac{E_\gamma}{3\,{\rm GeV}}\right)^{1/3}\left(\frac{B_{\rm d}}{B_{\rm c}}\right)^{1/3}\sin^{1/3}\theta_{kB}\,{\rm cm}. \tag{2}$$

The high-energy photons may be emitted along the magnetic field line by the relativistic particles, that is $\theta_{kB} \sim 0$, and hence they can initially propagate into the magnetosphere. However, because the field lines have a curvature and because the field lines are corotating with the magnetar, the collision angle increases as the photons propagate from the emission point. Under the approximation of the concentric circles of the magnetic field line, the collision angle θ_{kB} will develop as $\sin\theta_{kB} \sim s/\sqrt{R_{\rm c}^2 + s^2}$, where s is the propagation distance from the emission point and $R_{\rm c}$ is the curvature radius of the magnetic field line. Hence, the photons emitted blow $r \sim r_m$ will be converted into pairs after they propagate $s \sim R_{\rm c}$, where $\sin\theta_{kB}$ cannot be small.

The GeV γ-rays are also subject to the two photon pair-creation process with background soft X-ray field. Using typical observed luminosity $L_{\rm X} \sim 10^{35}\,{\rm erg\,s^{-1}}$ and temperature $kT \sim 0.5$ keV (e.g. Kuiper et al. 2006; den Hartog et al. 2008; Enoto et al. 2010), the number density can be estimated as $n_{\rm X} \sim L_{\rm X}/(4\pi r^2 c E_{\rm X}) \sim 3 \times 10^{20}(L_{\rm X}/10^{35}\,{\rm erg\,s^{-1}})(E_{\rm X}/0.5\,{\rm keV})^{-1}\,(r/10^6\,{\rm cm})^{-2}\,{\rm cm^{-3}}$. The optical depth $\tau \sim n_{\rm X}\sigma_{\gamma\gamma} r$, where $\sigma_{\gamma\gamma} \sim \sigma_{\rm T}/3$ is the pair-creation cross-section with $\sigma_{\rm T}$ being the Thomson cross-section, is below unity if GeV γ-rays are emitted above the radiation distance:

$$r_{\rm p} = 7\times10^7\left(\frac{L_{\rm X}}{10^{35}\,{\rm erg\,s^{-1}}}\right)\left(\frac{E_{\rm X}}{0.5\,{\rm keV}}\right)\,{\rm cm}. \tag{3}$$

Equations (2) and (3) imply that the critical radius $r_{\rm c}$ above which the produced GeV γ-rays can escape from the pair-creation processes is order of $r_{\rm c} \sim 5 \times 10^7$ cm.

3 EMISSION MODEL

3.1 The Alfvén wave excited by the crust fractures

Woods et al. (2005) proposed that there are two distinct types of magnetar's bursts, which were named Type A and Type B. Type A bursts are frequently seen in SGR bursts, in that they are uncorrelated with pulse phase and the energy emitted during primary burst peak is larger than the tail energy. Type B bursts, on the other hands, are correlated with the pulse phase and the energy of primary burst peak is smaller than the tail energy (see also Kaspi 2007; Scholz & Kaspi 2011; Dib et al. 2012). Woods et al. (2005) also speculated that the Type A and Type B bursts are triggered by the magnetospheric reconnection (Lyutikov 2003) and by the crust fractures (Thompson & Duncan 1995), respectively. Furthermore, several magnetars sometimes show timing glitches that accompany the radiative outbursts (Woods et al. 2004; Dib et al. 2012; İçdem, Baykal, Inam 2012; Pons & Rea 2012). In 2002 giant glitch of AXP 1E 2259+586, for example, the X-ray outburst were consisted of a rapidly decay emission in the first few hours with a released energy $\sim 10^{38}$ erg and a slow decay emission lasting several years with a released energy $> 10^{41}$ erg (Woods et al. 2004; Zhu et al. 2008), which are Type B burst. This giant glitch accompanying the radiative outburst is likely triggered by the crust fractures, which would simultaneously affect both superfluid core and the magnetosphere, and will inject an energy $\sim 10^{41\text{–}42}$ erg into the magnetosphere (Woods et al. 2004; Pons & Rea 2012).

In this paper, we consider the energy release caused by the crust cracking of the strong magnetic field, i.e. the Type B bursts. We assume that the magnetic field in the crust is deformed away from the equilibrium state by an amount of δB. The crust fracture will be occurred if the Maxwell stress $\delta B B_{\rm curst}/4\pi$, where $B_{\rm crust}$ is the equilibrium magnetic field in the crust, exceeds crustal elastic stress. The available magnetic energy density when the crust fracture is occurred may be expressed by (Thompson & Duncan 1995)

$$\frac{(\delta B)^2}{8\pi} \sim 2\pi\mu^2\epsilon_{\rm y}^2 B_{\rm crust}^{-2},$$

where μ is the shear modulus and $\epsilon_{\rm y}$ is the yield strain at which the crust cracks. The released magnetic energy is therefore estimated as

$$E_{\rm tot} = 2\times10^{42}\left(\frac{\mu}{10^{30}\,{\rm erg\,cm^{-3}}}\right)^2\left(\frac{\epsilon_{\rm y}}{2\times10^{-3}}\right)^2 \times\left(\frac{B_{\rm crust}}{10^{14}\,{\rm G}}\right)^{-2}\left(\frac{\ell}{10^5\,{\rm cm}}\right)^3\,{\rm erg}, \tag{4}$$

where ℓ is the typical size of the cracked platelet. Note that with a typical luminosity of the observed X-ray emissions $L_{\rm X} \sim 10^{34\text{–}35}\,{\rm erg\,s^{-1}}$, the emission will last a temporal scale of years, $\tau = E_{\rm tot}/L_{\rm X} \sim 10^{7\text{–}8}$ s.

The process of the γ-ray emission induced by the neutron star quake was discussed by Blaes et al. (1989), who investigated the possibility for the origin of γ-ray bursts. In their model, the neutron star quake will excite the oscillation of the magnetic field frozen into the star's crust, and the Alfvén waves carrying the released energy into the magnetosphere. The dissipation of wave energy will accelerate the electrons and/or positrons, which in turn radiate γ-rays.

In the magnetar model, it can be thought that the Alfvén wave is excited on the magnetic field lines anchored on the cracked platelet. If location of the cracking is close to the magnetic pole, a part of the released energy $E_{\rm tot}$ can be carried by the Alfvén waves that propagate into the outer magnetosphere $r \geq r_{\rm c} \sim 5 \times 10^7$ cm, where the γ-rays can escape from the pair-creation processes. Because the Alfvén wave propagates along the closed magnetic field lines, the wave may bounce many times between the footprints of the field lines. The time-averaged amplitude of the magnetic field

corresponding to the Alfvén wave energy density, $\sim E_{\rm tot}/R_{\rm c}^3$ may be described as

$$\delta B(R_{\rm s}) \sim 5\times10^{10}\left(\frac{E_{\rm tot}}{10^{42}\,{\rm erg}}\right)^{1/2}\left(\frac{R_{\rm c}}{2\times10^{7}\,{\rm cm}}\right)^{-3/2}{\rm G} \quad (5)$$

near the stellar surface.

As the Alfvén wave propagates from the stellar surface into outer magnetosphere, the amplitude will evolve as $\delta B(r)\propto A^{-1/2}(r)$, where $A(r)$ is the cross-section of the oscillating magnetic flux tube. Because the background dipole field is proportional to $B_{\rm d}(r)\propto A^{-1}(r)$, the ratio of the perturbed and background magnetic fields evolves with the radial distance as

$$\frac{\delta B(r)}{B_{\rm d}(r)} = \frac{\delta B(R_{\rm s})}{B_{\rm d}(R_{\rm s})}\left(\frac{B_{\rm d}(R_{\rm s})}{B_{\rm d}(r)}\right)^{1/2} \sim 10^{-3}\left(\frac{B_{\rm d}(R_{\rm s})}{B_{\rm d}(r)}\right)^{1/2}. \quad (6)$$

In the magnetosphere of magnetar, the speed of the Alfvén wave exceeds the speed of light, i.e.

$$v_{\rm A}\equiv\frac{B}{\sqrt{4\pi\rho}}\gg c, \quad (7)$$

where the ρ is the mass density. In the limit of $v_{\rm A}\gg c$, we can see that the required current density ($i_{\rm a}$) to support the propagation of the Alfvé wave at distance r is in order of (see Appendix A)

$$\frac{i_{\rm a}(r)}{\kappa i_{\rm GJ}(r)} \sim \frac{\omega\beta_{\rm co}(r)\delta B(r)}{\kappa\Omega B_{\rm d}(r)} \sim 10\beta_{\rm co}\left(\frac{\omega}{10^4\,{\rm Hz}}\right)\left(\frac{\Omega}{1\,{\rm Hz}}\right)^{-1} \times\left(\frac{\delta B(R_{\rm s})/B_{\rm d}(R_{\rm s})}{10^{-3}}\right)\left(\frac{B_{\rm d}(R_{\rm s})}{B_{\rm d}(r)}\right)^{1/2}, \quad (8)$$

where $i_{\rm GJ}=\Omega B/2\pi$ is the Goldreich–Julian current density, and ω is the typical shear frequency of the wave, which may be estimated as $\omega\sim\rho_{\rm crust}^{-1/2}\mu^{1/2}\ell^{-1}\sim10^4$ Hz with $\rho_{\rm crust}\sim5\times10^{11}\,{\rm g\,cm^{-3}}$ being the typical mass density in the crust. In addition, κ is the multiplicity.

We can see that in the limit of $v_{\rm A}\gg c$, the induced electric field is same order of magnitude as the perturbed magnetic field, $\delta E\sim\delta B$ (see Appendix A). Hence, the maximum magnitude of the induced electric potential due to perturbation of the magnetic field lines may be estimated as

$$\delta\Phi_{\rm p}\sim\delta\ell\times\delta B = 1.5\times10^{15}\left(\frac{\delta B(R_{\rm s})/B_{\rm d}(R_{\rm s})}{10^{-3}}\right) \times\left(\frac{\delta B(R_{\rm s})}{5\times10^{10}\,{\rm G}}\right)\left(\frac{\ell}{10^5\,{\rm cm}}\right){\rm V}, \quad (9)$$

where $\delta\ell$ is the displacement of footprints of the oscillating magnetic lines and was estimated as

$$\delta\ell\sim\frac{\delta B(R_{\rm s})}{B_{\rm d}}\ell\sim10^2\left(\frac{\delta B(R_{\rm s})/B_{\rm d}}{10^{-3}}\right)\left(\frac{\ell}{10^5\,{\rm cm}}\right){\rm cm}. \quad (10)$$

The maximum radiation power may be estimated as

$$L_{\rm r}\sim\delta\Phi_{\rm p}\,I\sim4\times10^{35}\left(\frac{\Omega}{1\,{\rm Hz}}\right)\left(\frac{\delta B(R_{\rm s})}{5\times10^{10}\,{\rm G}}\right)^2 \times\left(\frac{\ell}{10^5\,{\rm cm}}\right)^3\left(\frac{I}{I_{\rm GJ}}\right){\rm erg\,s^{-1}}, \quad (11)$$

where I is the total current and $I_{\rm GJ}\sim i_{\rm GJ}\ell^2$.

3.2 Acceleration and GeV emission process

In Fig. 1, we illustrate the schematic view of our model for the particle acceleration and GeV emissions in the magnetosphere of the magnetar. If the magnetic field cracks the platelet near the magnetic axis, the oscillating magnetic flux tube will extend beyond $r_{\rm c}\sim5\times10^7$ cm. We will argue that the particles are accelerated by the Alfvén wave, which is excited by the crust cracking of the magnetic field. It will be possible that the energy dissipation of the Alfvén wave accelerates the electrons and/or positrons to a Lorentz factor above $\Gamma\sim10^7$. The curvature radiation process of the accelerated particle can produce GeV γ-rays. The GeV γ-rays emitted above $r_{\rm c}\sim5\times10^7$ cm will escape from the pair-creation process and may be observed as the pulsed emissions. In this section, we will discuss possible particle acceleration processes related to the propagation of the Alfvén wave.

First, if the co-rotation motion is ignored $\boldsymbol{v}_{\rm co}=0$, the induced electric field $\delta\boldsymbol{E}$ and the background magnetic field are a mutually orthogonal and hence no electric field along the background magnetic field is induced. However, under the presence of the co-rotation motion of the plasmas, such orthogonality breaks down, and the electric field and the current along the background magnetic field line are induced (Kojima & Okita, 2004). The typical strength of the electric field along the background magnetic field line, $\delta E_{||}$, is described as (see Appendix A)

$$\delta E_{||}(r)\sim\beta_{\rm co}\delta B(r). \quad (12)$$

If the Lorentz factor of particle is determined by the balancing the between the electric force and the curvature radiation reaction force, we obtain

$$\Gamma(r)\sim\left(\frac{3R_{\rm c}^2}{2e}\delta E_{||}\right)^{1/4}\sim3.5\times10^7\left(\frac{\delta B(R_{\rm s})}{5\times10^{10}\,{\rm G}}\right)^{1/4} \times\left(\frac{\beta_{\rm co}}{10^{-3}}\right)^{1/4}\left(\frac{r}{10^8\,{\rm cm}}\right)^{-3/8}\left(\frac{R_{\rm c}}{10^8\,{\rm cm}}\right)^{1/2}, \quad (13)$$

where $R_{\rm c}$ is the curvature radius of the dipole field. We can see that the typical energy of the curvature photons becomes several GeV, i.e.

$$E_{\rm c}=\frac{3}{4\pi}\frac{hc\Gamma^3}{R_{\rm c}}\sim8\left(\frac{\Gamma}{3\times10^7}\right)^3\left(\frac{R_{\rm c}}{10^8\,{\rm cm}}\right)^{-1}{\rm GeV}. \quad (14)$$

Secondly, the deficiency of the current (or charge) to support the frozen in condition, $\boldsymbol{E}+\boldsymbol{\beta}\times\boldsymbol{B}=0$, could induce the electric field along the magnetic field (see also Blaes et al. 1989; Fatuzzo & Melia 1993; Thompson 2006). We can see in equation (8) that the required current to support the propagation of the Alfvén wave easily exceeds the Goldreich–Julian current. Furthermore, the typical charge density of the unperturbed particles in the closed field region will be coincide with the Goldreich–Julian charge density of the dipole field, that is $\rho_{\rm e}=-\boldsymbol{\Omega}\cdot\boldsymbol{B}_{\rm d}/2\pi c$. If the Alfvén wave propagates into outer magnetosphere, however, the perturbation of the magnetic field line changes the local Goldreich–Julian charge density as

$$\rho_{\rm GJ,1}=-\frac{\boldsymbol{\Omega}\cdot(\boldsymbol{B}_{\rm d}+\delta\boldsymbol{B})}{2\pi c}=\rho_{\rm GJ,0}+\delta\rho_{\rm GJ}, \quad (15)$$

where $\delta\rho_{\rm GJ}\equiv-\boldsymbol{\Omega}\cdot\delta\boldsymbol{B}/2\pi$. The electric field along the magnetic field line then will be induced, if the primary particles could not supply the required charge density $\rho_{\rm GJ,1}$. The particles could be accelerated at the 'charge-starved' region up to the Lorentz factor $\Gamma\sim10^7$, such as the particle acceleration process of the γ-ray pulsars (e.g. Wang, Takata & Cheng 2010). The accelerated particles will emit the γ-rays via the curvature radiation process. Most of the γ-rays produced below $r\sim r_{\rm c}$ will be converted into electron and positron pairs through the pair-creation processes. Because the GeV γ-rays are emitted along the magnetic field lines, the pairs

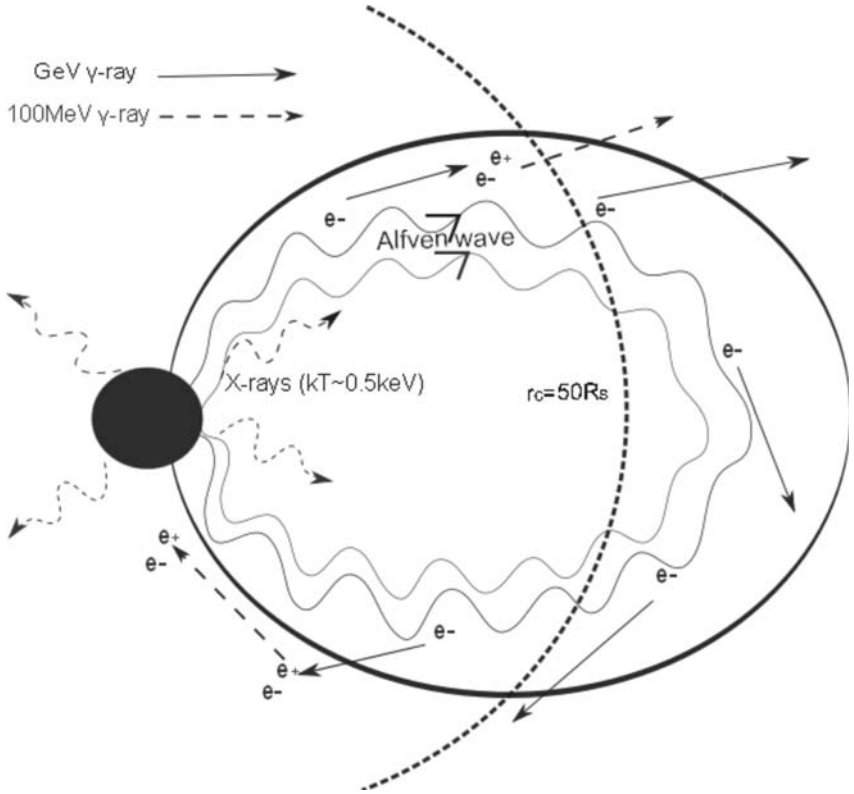

Figure 1. Schematic view for the pulsed GeV γ-ray emissions from magnetars. The figure represents snap shot at which the Alfvén wave propagates from the north pole to south pole. The GeV γ-rays produced above $r_{\rm c} \sim 5 \times 10^7$ cm can escape from the pair-creation process. The created pairs below $r_{\rm c}$ eventually heat up the stellar surface and will contribute to the soft X-ray emissions from the stellar surface. Some of outwardly propagating 100 MeV photons emitted via the synchrotron radiation of the first generation of pairs will also escape from the pair-creation process, if they are produced beyond $r_{c1} \sim 10^7$ cm.

are produced at the convex side of the magnetic field line on which primary γ-rays were emitted (cf. Fig. 1). The multiplicity is roughly estimated as $\kappa \sim \lambda\, e\delta\Phi/\Gamma m_{\rm e}c^2 = 2 \times 10^3 (\Phi/10^{15}\ {\rm V})(\Gamma/3 \times 10^7)^{-1}$ with $\lambda \sim r_{\rm c}/(5 \times 10^8)\,{\rm cm} \sim 0.1$ being the fractional power spent below $r \sim r_{\rm c}$. A fraction of the created pairs is probably charge separated, and will produce the required current (8) to support the propagation of the Alfvén wave.

Finally, if the Alfvén wave does not efficiently dissipate along the background magnetic field lines, the ratio of the amplitude of the Alfvén wave to the dipole field will evolve as $\delta B(r)/B_{\rm d}(r) \propto 10^{-3}(B_{\rm d}(R_{\rm s})/B_{\rm d}(r))^{1/2}$, as equation (6) shows. Hence, we find that the fractional perturbation of the magnetic field becomes order of unity at the radial distance $r \sim 10^8[\delta B(R_{\rm s}))/10^{-3}B_{\rm d}(R_{\rm s})]^{-2/3}$ cm. Because the induced electric field is same order of magnitude as the perturbed magnetic field, $\delta E \sim \delta B$, the total electric field is of order of the magnetic field $|E| \sim |B|$, where conversion from the electromagnetic energy into the particles energy could be possible (Beskin & Rafikov 2000). When the non-linear term becomes to be important, by whatever process, a substantial part of the wave energy is probably converted into the electron/positron energy, which in turn radiate the GeV γ-rays.

In any acceleration processes process discussed above, the typical Lorentz factor will be characterized by

$$\Gamma_{\rm max} \sim \left(\frac{3R_{\rm c}^2}{2e}E_{||}\right)^{1/4} = 3 \times 10^7 \left(\frac{R_{\rm c}}{10^8\ {\rm cm}}\right)^{1/4} \left(\frac{L}{R_{\rm c}}\right)^{-1/4} \times \left(\frac{\delta B(R_{\rm s})}{5 \times 10^{10}\ {\rm G}}\right)^{1/2} \left(\frac{B_{\rm d}(R_{\rm s})}{10^{14}\ {\rm G}}\right)^{-1/4} \left(\frac{\ell}{10^5\ {\rm cm}}\right)^{1/4}, \quad (16)$$

where we used typical electric field $E_{||} = \delta\Phi_{\rm p}/L$ with L being the arc length of the acceleration region along the magnetic field line.

3.3 Incident X-ray/soft γ-ray emission

In the present scenario, the relativistic electrons/positrons, which were accelerated in outer magnetosphere, will be return to the stellar surface, because they migrate along the closed magnetic field lines. Below $r_{\rm c} \sim 5 \times 10^7$ cm, most of γ-rays emitted by incoming particles will be converted into electron/positron pairs via the pair-creation process with the soft X-rays and/or magnetic field. Those pairs are mainly produced at the convex side of the magnetic field lines, on which the primary γ-rays were emitted. New born pairs will lose their energy via the synchrotron radiation and/or the resonant Compton scattering, in which the Compton scattering is occurred in the resonant energy $\Gamma_{\rm e\pm}E_{\rm X} \sim \hbar e B_{\rm d}(r)/m_{\rm e}c$, with $\Gamma_{\rm e\pm}$ being Lorentz factor of the pairs. Those photons could also make new pairs. This cascade process will produce lots of low-energy electron/positron pairs near the stellar surface. The incoming pairs will carry the energy of $L_{\rm e\pm} \sim \lambda L_{\rm r} \sim 4 \times 10^{34}\ {\rm erg\ s^{-1}}$.

The incoming pairs eventually reach the stellar surface and heat up the stellar surface. The temperature of the heated platelet may be $k_{\rm B}(L_{e\pm}/\ell^2\sigma_{\rm SB})^{1/4} \sim 2(L_{\rm e\pm}/10^{35}\ {\rm erg\ s^{-1}})^{1/4}\ (\ell/10^5\ {\rm cm})^{-1/2}$ keV, with $k_{\rm B}$ being the Boltzmann constant and $\sigma_{\rm SB}$ Stephan–Boltzmann constant. These hard X-rays emitted from the heated platelet may be too high to escape from the resonant Compton scattering near the stellar surface. The scattered X-rays will be redistributed on the stellar surface, and emerge as the soft X-ray emission with a temperature of $kT_{\rm s} \sim k(L_{\rm e\pm}/\triangle\Omega R_{\rm s}^2\sigma_{\rm SB})^{1/4} \sim$

$0.6(L_{e\pm}/10^{35}\,\mathrm{erg\,s^{-1}})\triangle\Omega^{-1/4}$ keV, where $\triangle\Omega$ is the solid angle of the emission. It is also possible that because some fraction of the incoming pairs will be created outside the oscillating magnetic field lines that connect to the cracked platelet, the typical size of the heated surface by the incoming particles is larger than ℓ. In the present scenario, hence, the temperature of the intrinsic emissions from the heated surface by the incoming particles will be $kT_s \sim 0.5$ keV.

For 'outwardly' propagating GeV γ-rays produced near but below $r \sim 5 \times 10^7$ cm, the cascade process will not develop to reduce the photon energy to ∼MeV, and stop after producing the first or second generation of pairs. For example, the first generation of pairs produced by the magnetic pair-creation process will emit the synchrotron photons with an energy $\sim E_\gamma/20 \sim 100$ MeV, where E_γ is the primary GeV γ-ray produced by the curvature radiation (Cheng, Gil & Zhang 1998). The outwardly propagating photons with ∼100 MeV will escape from the magnetic pair-creation processes if they are produced beyond $r_{c1} \sim 10^7$ cm (cf. equation 1). Between $r_{c1} \sim 10^7$ cm and $r_c \sim 5 \times 10^7$ cm, hence, outwardly propagating ∼100 MeV photons emitted by the first generation pairs will escape from the magnetosphere of the magnetars, and will be contribute to the observed spectrum. We expect that the luminosity of this component will be $L_{100\,\mathrm{MeV}} \sim \lambda L_r$, where $\lambda \sim (r_c - r_{c1})/(5 \times 10^8\,\mathrm{cm}) \sim 0.1$.

3.4 Pulse profiles

In this section, we discuss the expected pulse profiles of the γ-ray emissions. We refer the previous studies (e.g. Takata, Chang & Cheng 2007) for the calculation of the pulse profile. We apply the vacuum rotating dipole field as the magnetic field in the magnetosphere. We describe the polar angle of the magnetic field lines at the stellar surface with $a \equiv \theta(\phi)/\theta_p(\phi)$, where θ_p is the polar angle of the last-open field line and ϕ is the magnetic azimuth. The open and closed magnetic field lines correspond to $a < 1$ and $a > 1$, respectively. Because the polar cap radius is only ∼1 per cent of the stellar radius, it is likely that the cracking platelet by the magnetic field is occurred at the closed field line region. As we discuss in Section 2, the GeV γ-rays can escape from the pair-creation process if they are produce beyond $r \sim 5 \times 10^7$ cm from the stellar surface. In this section, hence, we apply $a = 16$, in which the magnetic field lines extend up to $r \sim 5 \times 10^8$ cm, as the main emission region. The width of the emitting magnetic flux tube in the azimuthal direction is assumed to be $\delta\phi \sim 1$ rad, because the typical size of cracked platelet is $R_s\theta_c\delta\phi \sim \ell \sim 10^5$ cm, where $\theta_c \sim \sqrt{R_s/r_c} \sim 0.1$ rad is the polar angle of the magnetic field lines that extend beyond $r \sim r_c \sim 5 \times 10^7$ cm.

We assume a constant emissivity along the magnetic field line, and at each point we express the opening angle of the γ-ray cone as

$$\theta_{\mathrm{GeV}} \sim \frac{\delta B(r)}{B_d(r)} = 10^{-3}\left(\frac{r}{R_s}\right)^{3/2}, \tag{17}$$

which represents the effect of the oscillation of the magnetic field lines, on which the Alfvén wave propagates (cf. equation 6). The direction of the centre of the radiation cone coincides with the direction of the background vacuum dipole field. Because the Alfvén wave propagates along the closed magnetic field lines, the wave may bounce many times between the footprints of the field lines. The crossing time-scale of the Alfvén wave, $\tau_c \sim 10^8\,\mathrm{cm}/v_A \sim 0.01$ s with $v_A \sim c$ being the speed of the Alfvén wave, is much shorter than the rotation period. To calculate the pulse profile, hence, we take into account the γ-ray emissions from both particles migrating from north to south poles and from south to north poles. The inwardly propagating γ-rays may be absorbed by the pair-creation process with the background X-rays and/or the magnetic field if they pass through near the stellar surface. To take into account this effect, we ignore the contribution from the inwardly propagating γ-rays that pass through the region $r < 5 \times 10^7$ cm.

The predicted light curves for the inclination angle $\alpha = 60^\circ$ are summarized in Figs 2 and 3, which are the sky-photon-mapping and the calculated light curves, respectively. We assume that the azimuthal angle of the centre of the emitting magnetic flux tube, which has a width $\delta\phi \sim 1$ rad, is $\phi_c = 0^\circ, 90^\circ, 180^\circ$ and 270°. In Fig. 2, the whiteness refers the emissivity of the radiation on (ξ, Φ) plane, where ξ and Φ are the Earth viewing angle and the rotation phase, respectively. The brighter region (e.g. $\Phi \sim 0.2$ and $\xi \sim 100^\circ$ in the panel for $\phi_c = 90^\circ$) corresponds to the rotation phase at which both radiations produced by the particles migrating from north to south poles and from south to north poles contribute to the observed emissions, while the dark region (e.g. $\Phi \sim 0.75$ and $\xi \sim 80^\circ$ in the panel for $\phi_c = 90^\circ$), both emissions passes through the region $r \leq 5 \times 10^7$ cm and do not contribute to the observed emissions.

In Fig. 3, from top to bottom, the calculated light curves are for $\xi = 30^\circ, 60^\circ, 120^\circ$ and 150°, respectively. We can see in Fig. 3 that the calculated light curves have in general broad peak in one-rotation period with sometimes sharp peaks (e.g. $\phi_c = 90^\circ$ and $\xi = 120^\circ$). For the emission from the closed field lines, the special relativistic effects can be ignored, while it becomes important to explain the sharp and narrow pulse profiles of canonical γ-ray pulsars (Romani & Yadigaroglu 1995), in which the observed emissions are produced on the open field line region. In the present scenario, on the other hand, the sharp peak appears if the radiations from both kinds of particles migrating towards south pole and towards north pole are observed simultaneously.

3.5 Spectrum

To calculate the typical spectrum, we assume that the acceleration region extends beyond $r \geq 10^7$ cm and all of GeV γ-rays emitted above $r_c = 5 \times 10^7$ cm can escape from the pair-creation process. Between $r_{c1} \sim 10^7$ cm and r_c, furthermore, all synchrotron photons emitted by the outwardly migrating pairs, which were produced by outwardly propagating γ-rays, can escape from the pair-creation processes, as discussed in Section 3.3. The spectrum of the curvature radiation at each calculation grid is expressed as

$$P_c(E_\gamma) = \frac{\sqrt{3}e\Gamma_p}{hcR_c}F(\chi)j_aA, \tag{18}$$

where $\chi = E_\gamma/E_c$ with $E_c = 3hc\Gamma^3/4\pi R_c$ and

$$F(\chi) = \chi\int_\chi^\infty K_{5/3}(\xi)\,\mathrm{d}\xi,$$

where $K_{5/3}$ is the modified Bessel function of order 5/3. In addition, j_a is the current density and A is the cross-section of the grid perpendicular to the dipole field. In this section, we assume the Goldreich–Julian value, $j_a(r) = \Omega B_d(r)/2\pi$, for the current density. We assume that the Lorentz factor of the accelerated particles is given by equation (16).

The synchrotron radiation of the outwardly migrating pairs produced between r_{c1} and r_c (cf. Section 3.3) may be described by

$$P_s(E_s) = \frac{\sqrt{3}e^3B\sin\theta_p}{m_ec^2h}\int\frac{\mathrm{d}N_e}{\mathrm{d}E_e}F(\zeta)\,\mathrm{d}E_e, \tag{19}$$

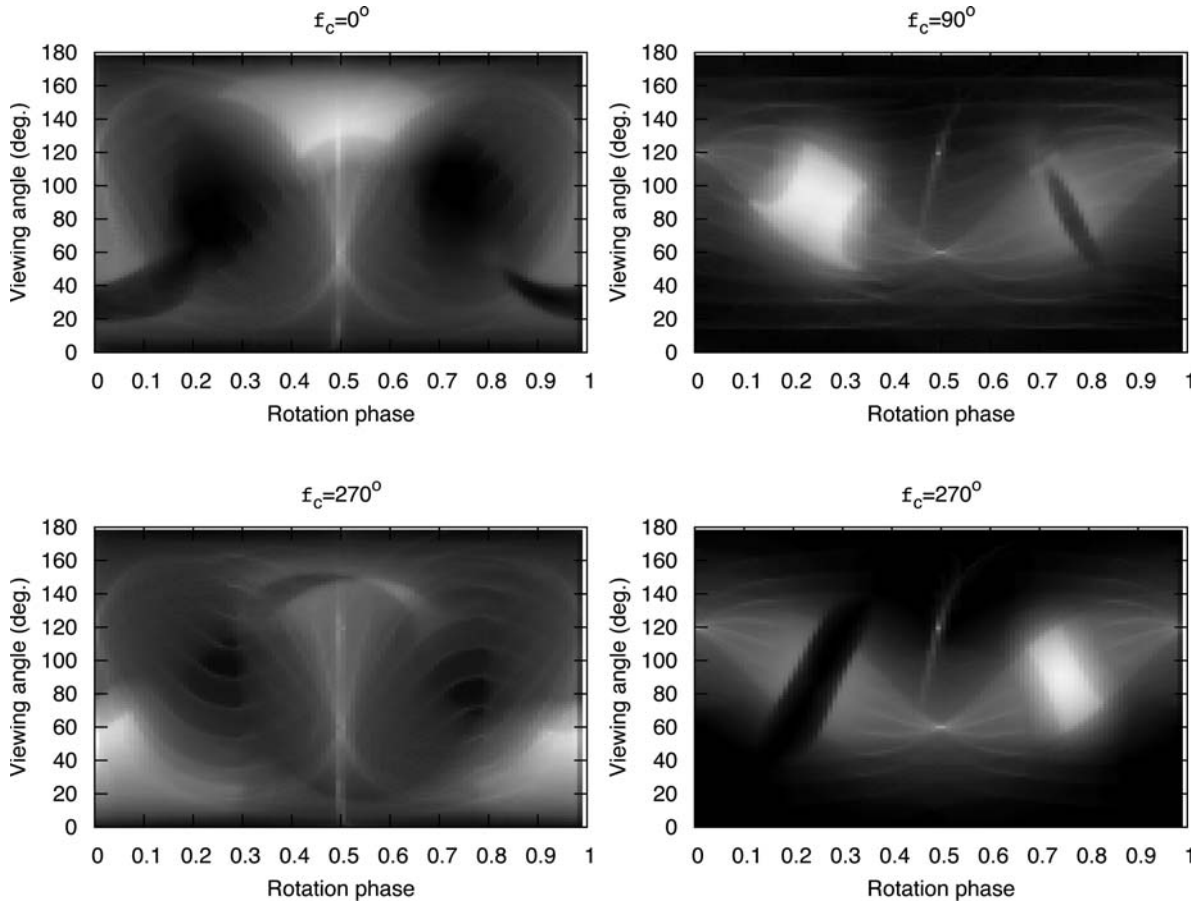

Figure 2. Sky maps of GeV γ-ray emissions for the inclination angle of $\alpha = 60^\circ$ and $a = 16$. The centre of the emitting magnetic flux tube is $\phi_c = 0^\circ$ (upper left), 90° (upper right), 180° (lower left) and 270° (lower right), respectively. The whiteness refers the emissivity of the radiation.

where $\zeta = E_s/E_{syn}$ with $E_{syn} = 3\Gamma_{e\pm}^2 ehB_d(r)\sin\theta_p/4\pi m_e c$ and θ_p the pitch angle. The distribution of the pairs under the steady condition may be described as

$$\frac{dN_e}{dE_e} \sim \frac{P_c(E_\gamma)}{\dot{E}_{syn}}, \quad \Gamma_{e\pm,min} \le \Gamma_{e\pm} \le E_\gamma/2m_e c^2, \tag{20}$$

where $\dot{E}_{syn} = 2e^2B^2\sin^2\theta_p\Gamma_{e\pm}^2/3m^2c^5$ is the energy loss rate of the synchrotron radiation. The minimum Lorentz factor of the pairs is $\Gamma_{e\pm,min} \sim 1/\sin\theta_p \sim m_e c^2 B_c/(\chi E_\gamma B_d(r))$.

Fig. 4 summarizes typical spectra predicted by the present scenario. In Fig. 4, we have used $\alpha = 60^\circ$ for the inclination angle, $a = 16$ for the magnetic surface of the typical emission region and $\phi_c = 0^\circ$ for the azimuthal angle of the centre of oscillating magnetic flux tube. In Fig. 4, the right- and left-hand panels show the dependency of the spectra of the curvature radiation on the released energy (E_{tot}) and on the global dipole field ($B_d(R_s)$), respectively. The results are for $\Omega = 1\,s^{-1}$ and $\ell = 10^5$ cm. We find in Fig. 4 that the luminosity is proportional to the released total energy because $L_\gamma \propto \delta B^2(R_s) \propto E_{tot}$, as indicated by equation (11). As we can see in Fig. 4, the typical energy of the curvature spectrum increases with the released energy, i.e. $E_c \propto \delta B^{3/2}(R_s) \propto E_{tot}^{3/4}$ (cf. equation 14). In the right-hand panel of Fig. 4, we see that the typical energy of the curvature radiation decreases with increase of the magnetic field. This is because the displacement of the footprints of the oscillating magnetic field lines becomes smaller for stronger background magnetic field, as equation (10) indicates. The decrease of the displacement implies the decrease of the potential drop (equation 9) and hence the decrease of the typical energy of the curvature radiation, $E_c \propto B_d^{-3/4}(R_s)$ (equation 14).

In Fig. 5, we present the predicted spectrum in wide energy band using the parameters of AXP 1E 2259+586 ($\Omega \sim 0.9\,s^{-1}$ and $B_d(R_s) \sim 10^{14}$ G). AXP 1E 22459+586 has shown frequent glitches, which sometimes accompany the X-ray outbursts. Furthermore, the GeV γ-ray emissions in the direction of CTB 109, which will be associated with AXP 1E 22459+586, were founded in the *Fermi* data (Castro et al. 2012). Although the origin from SNR has been suggested, the possibility of the emissions from AXP 1E 22459+586 has not been ruled out yet.

The model spectrum in Fig. 5 is result for $E_{tot} = 2 \times 10^{42}$ erg, $\ell = 5 \times 10^4$ cm, $\phi_c = 0^\circ$ and $a = 13$. The solid line and dashed line are spectra of the curvature radiation above $r \ge 5 \times 10^7$ cm and in the range $10^7 \le r \le 5 \times 10^7$ cm, respectively. The dotted line represents the synchrotron spectrum from the first generation of pairs, if all outgoing photons above 1 GeV emitted in the range $10^7 \le r \le 5 \times 10^7$ cm (dashed line) are absorbed by the magnetic field (cf. Section 3.3). The measured spectrum is represented by the filled circles of Fig. 5. We can seen in Fig. 5 that if the observed GeV emissions would be originated from the magnetosphere, the observed flux level could be explained by the present scenario with the total released energy of $E_{tot} = 2 \times 10^{42}$ erg and the typical size of the cracking platelet of $\ell \sim 5 \times 10^4$ cm, respectively. However, the present model can reproduce only emissions below $\sim$10 GeV, as Fig. 5 shows. Above 10 GeV, the present model expects that the emissions from SNR dominate the magnetospheric emissions.

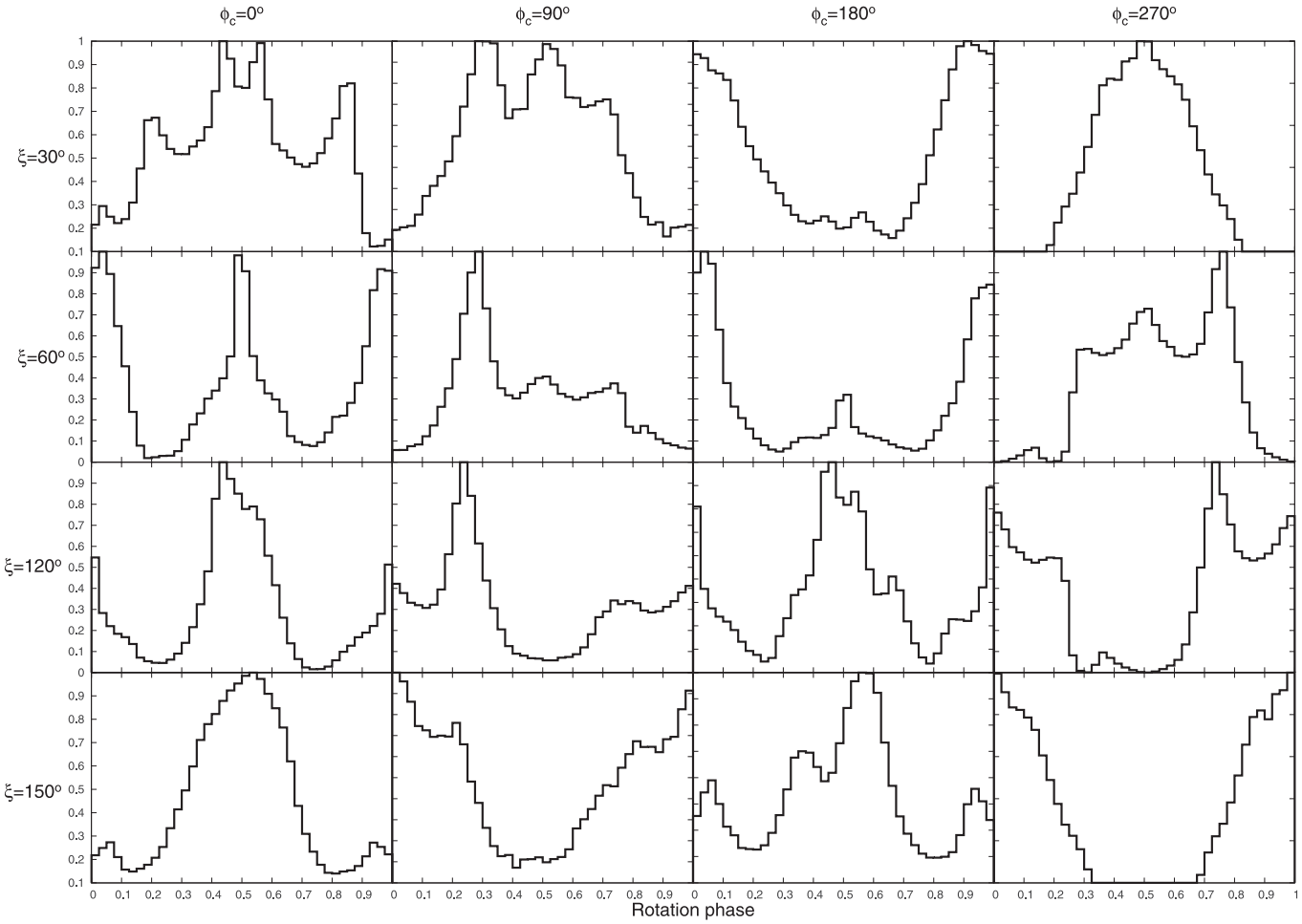

Figure 3. The calculated light curves for the inclination angle of $\alpha = 60^\circ$ and $a = 16$. From the top to bottom, the calculated light curves are for $\xi = 30^\circ, 60^\circ, 120^\circ$ and 150°, respectively.

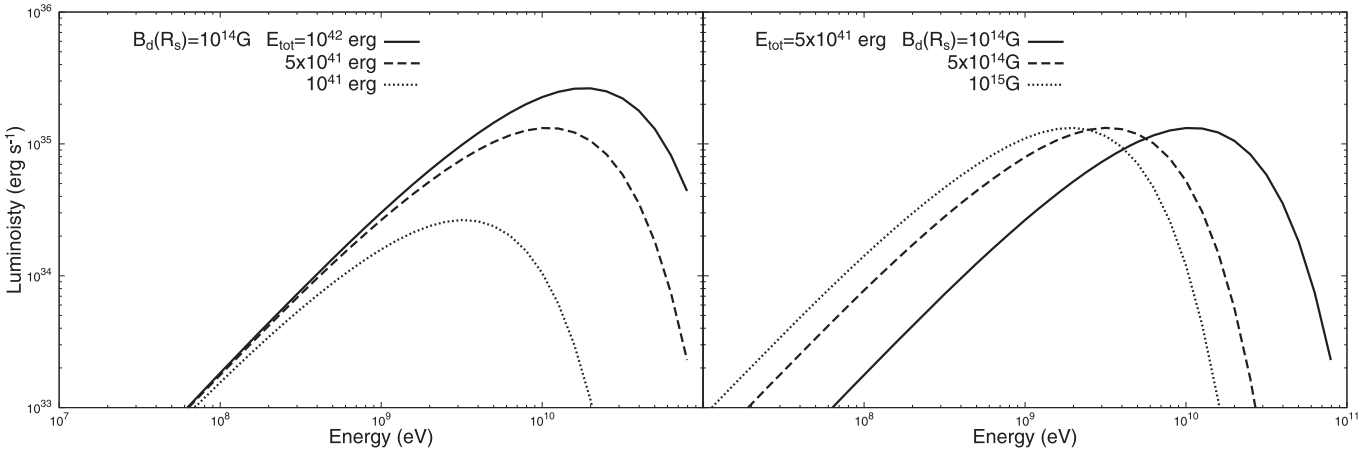

Figure 4. Spectrum of the curvature radiation from the oscillating magnetic flux tube. The results are for $\alpha = 60^\circ$, $\Omega = 1\,\mathrm{s}^{-1}$, $\phi_c = 0^\circ$ and $a = 16$. The acceleration region extends beyond $r \geq 10^7$ cm and the all emissions above (below) $r = 5 \times 10^7$ cm can (cannot) escape from the pair-creation processes. Left: $B_d(R_s) = 10^{14}$ G. The solid, dashed and dotted lines are result for $E_{tot} = 10^{42}$, 5×10^{41} and 10^{41} erg, respectively. Right: $E_{tot} = 5 \times 10^{41}$ G. The solid, dashed and dotted lines are result for $B_d(R_s) = 10^{14}$, 5×10^{14} and 10^{15} G, respectively.

The synchrotron radiation near $r_c \sim 5 \times 10^7$ cm (dotted line) can extend down to hard X-ray bands, but its flux level is well below the persistent X-ray emissions measured by *RXTE* (filled triangles; Kuiper et al. 2006). Hence, it will be difficult to observe the synchrotron radiation in the outer magnetosphere.

4 DISCUSSION

We have discussed possible scenario for the pulsed GeV γ-ray radiation in outer magnetosphere of the magnetar. The GeV γ-rays will escape from the pair-creation process if the emission process

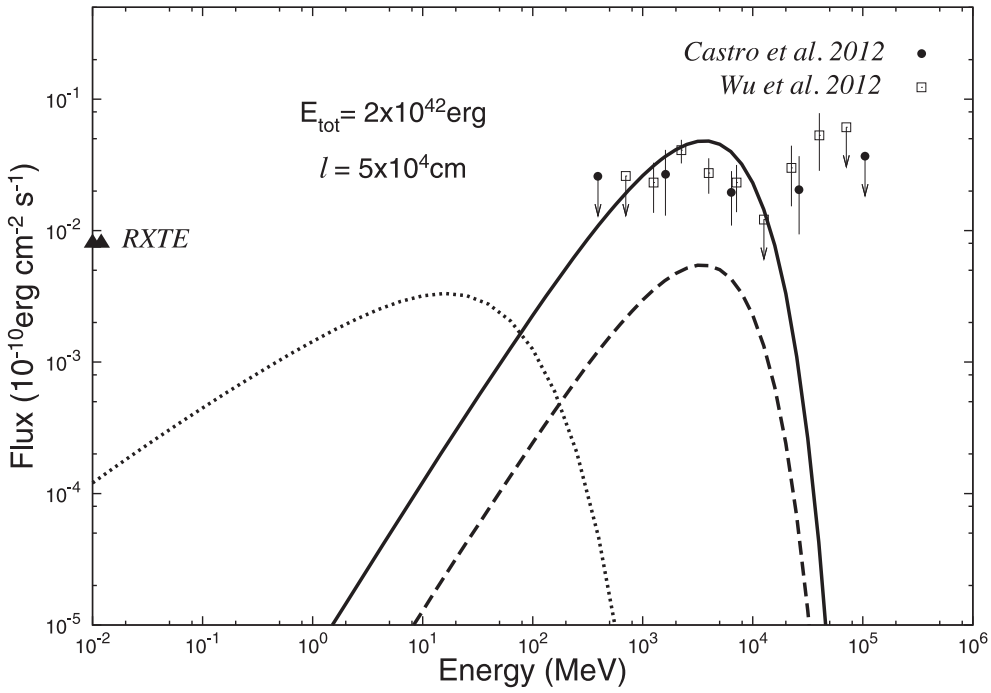

Figure 5. The spectrum of AXP 1E 2259+586. The solid and dashed lines are curvature radiation above and below $r = 5 \times 10^7$ cm, respectively. The results are for $E_{\rm tot} = 2 \times 10^{42}$ erg and $\ell = 5 \times 10^4$ cm. The dotted line is spectrum of the synchrotron radiation from the first generation of the pairs produced $10^7 \leq r \leq 5 \times 10^7$ cm, if all curvature photons above 1 GeV (dashed line) are absorbed by magnetic field. The data are taken from Castro et al. (2012) and from Wu et al. (2012) for the *Fermi* and from Kuiper et al. (2006) for the *RXTE*, respectively.

is occurred beyond $r_{\rm c} \sim 5 \times 10^5$ cm. In the present scenario, the Alfvén wave carries the magnetic energy released by the crust cracking of the magnetic field into outer magnetosphere $r \geq r_{\rm c}$ along the background magnetic field. The oscillation of the magnetic field induces the available potential drop $\delta\Phi_{\rm p} \sim 10^{15}$ V, which can accelerate the electrons and/or positrons to the Lorentz factor $\Gamma \sim 10^7$. The curvature radiation at the outer magnetosphere can produce GeV γ-rays.

The pulsed GeV γ-ray radiation from the magnetars have not been reported yet, although the predicted luminosity $L_\gamma \sim 10^{35}$ erg s^{-1} may be large enough to detect pulsed GeV γ-rays by the *Fermi* telescope. However, several reasons can be raised to explain the non-detection of the pulsed GeV emissions from the magnetars. First, the magnetars are in general located at the Galactic plane, the background radiation may prevent the detection of the pulsed radiation. Secondly, the magnetars have shown frequent glitches that are sudden changes in frequency and/or frequency derivative (İçdem et al. 2012). Hence the timing parameters of the magnetars are very unstable, which makes even harder to detect the pulsed period in the *Fermi* data. Thirdly, it has become clear that the magnetars are associated with the SNRs (Allen & Horvath, 2004; Gaensler et al. 2005; Halpern & Gotthelf 2010). It is possible that γ-ray emissions from SNRs dominate the pulsed emissions in the data. Recent *Fermi* observations have revealed properties of the GeV radiations from SNRs (Abdo et al. 2009, 2010, 2011). For the young SNRs, the accelerated electrons at the forward shock may produce the GeV radiations through the inverse-Compton process, while for middle age SNRs, the interaction between the accelerated protons and ambient molecular clouds produces the bright GeV radiations via the π^0 decay process.

We note that the typical luminosity of GeV radiation of SNRs is order of 10^{34-35} erg s^{-1}, which is same order of magnitude predicted by the present magnetospheric emission model. Hence, it would be possible that the GeV emissions in the direction of magnetars are composed of the emissions from SNRs and magnetospheres. The pulsed radiation predicted by the present scenario will change its luminosity level $L_\gamma \sim 10^{34-35}$ erg s^{-1} at a temporal scale of years after the energy injection into the magnetosphere, while the SNR's emission will be stable. Hence, a temporal behaviour of the observed GeV emissions will discriminate between the two components.

Finally, we note that it has been proposed that the glitch of normal pulsars is caused by unpinning of the superfluid vortices from the lattice (Alpar 2001). The energy released by the glitch is deposited at inner crust, and most of energy is dissipated to heat up the entire star (Tang & Cheng 2001). The increases of the surface X-ray emission may affect the γ-ray emission because of the photon–photon pair-creation process. With a typical released energy $\sim 10^{42}$ erg, the glitch can increase surface X-ray emissions by a factor of 2–3 if the core temperature is $T_{\rm c} \sim 10^7$ K for old pulsars or only a few per cent if $T_{\rm c} \sim 10^8$ K for young pulsars (Tang & Cheng 2001). Hence, it is expected such small change of the surface emission does not change much the γ-ray fluxes for young pulsars, e.g. Crab and Vela. For the magnetar case, on the other hand, the cracking of the outer crust could trigger the glitches that accompany the radiative outburst. A part of the released energy is carried into the magnetosphere via Alfvén waves, and may be used to accelerate the particles, which results in the GeV γ-ray emissions.

ACKNOWLEDGEMENTS

We express our appreciation to an anonymous referee for useful comments. We thank M. Ruderman, S. Shibata, A. H. Kong, D. Hui and J. H. K. Wu for the useful discussions. This work was supported by a GRF grant of Hong Kong Government under HKU700911P.

REFERENCES

Abdo A. A. et al., 2009, ApJ, 706, L1
Abdo A. A. et al., 2010, Sci, 327, 1103
Abdo A. A. et al., 2011, ApJ, 734, 28
Allen M. P., Horvath J. E., 2004, ApJ, 616, 346
Alpar M. A., 2001, preprint (astro-ph/0112306)
Baring M. G., Harding A. K., 2007, Ap&SS, 308, 109
Beloborodov A. M., 2013, ApJ, 762, 13
Beloborodov A. M., Thompson C., 2007, ApJ, 657, 967
Beskin V. S., Rafikov R. R., 2000, MNRAS, 313, 445
Blaes O., Blandford R., Goldreich P., Madau P., 1989, ApJ, 343, 839
Castro D., Slane P., Ellison D. C., Patnaude D. J., 2012, ApJ, 756, 88
Cheng K. S., Zhang L., 2001, ApJ, 562, 918
Cheng K. S., Gil J., Zhang L., 1998, ApJ, 493, L35
den Hartog P. R., Kuiper L., Hermsen W., Kaspi V. M., Dib R., Knödlseder J., Gavriil F. P., 2008, A&A, 489, 245
Dib R., Kaspi V. M., Scholz P., Gavriil F. P., 2012, ApJ, 748, 3
Enoto T. et al., 2010, ApJ, 715, 665
Fatuzzo M., Melia F., 1993, ApJ, 407, 680
Fernández R., Thompson C., 2007, ApJ, 660, 615
Gaensler B. M., McClure-Griffiths N. M., Oey M. S., Haverkorn M., Dickey J. M., Green A. J., 2005, ApJ, 620, L95
Halpern J. P., Gotthelf E. V., 2010, ApJ, 725, 1384
Harding A. K., Lai D., 2006, Rep. Progress Phys., 69, 2631
İçdem A., Baykal A., Inam Ç. S., 2012, MNRAS, 419, 3109
Kaspi V. M., 2007, Ap&SS, 308, 1
Kojima Y., Okita T., 2004, ApJ, 614, 922
Kuiper L., Hermsen W., den Hartog P. R., Collmar W., 2006, ApJ, 645, 556
Lyutikov M., 2013, MNRAS, 346, 540
Mereghetti S., 2008, A&AR, 15, 225
Pons J. A., Rea N., 2012, ApJ, 750, L6
Rea N., Zane S., Turolla R., Lyutikov M., Götz D., 2008, ApJ, 686, 1245
Romani R. W., Yadigaroglu I.-A., 1995, ApJ, 438, 314
Ruderman M., Sutherland P. G., 1975, ApJ, 196, 51
Scholz P., Kaspi V. M., 2011, ApJ, 739, 94
Takata J., Chang H.-K., Cheng K. S., 2007, ApJ, 656, 1044
Tang A. P. S., Cheng K. S., 2001, ApJ, 549, 1039
Thompson C., 2006, ApJ, 651, 333
Thompson C., Duncan R. C., 1995, MNRAS, 275, 255
Thompson C., Lyutikov M., Kulkarni S. R., 2002, ApJ, 574, 332
Wang Y., Takata J., Cheng K. S., 2010, ApJ, 720, 178
Woods P. M., Thompson C., 2006, in Lewin W. H. G., van der Klis M., eds, Compact Stellar X-Ray Sources. Cambridge Univ. Press, Cambridge, p. 547
Woods P. M. et al., 2004, ApJ, 605, 378
Woods P. M. et al., 2005, ApJ, 629, 985
Wu J. H. K. et al., 2012, in van Leeuwen J., ed., Proc. IAU Symp. 291, Neutron Stars and Pulsars: Challenges and Opportunities after 80 Years, preprint (arXiv:1210.5422)
Zhu W., Kaspi V. M., Dib R., Woods P. M., Gavriil F. P., Archibald A. M., 2008, ApJ, 686, 520

APPENDIX A: PROPAGATION OF ALFVéN WAVE

Within the frame work of a simple geometry of the corotating magnetosphere (cf. Fig. A1), we discuss the Alfvén wave propagating along the magnetic field line. We define the z-axis as the spin axis, and assume a uniform magnetic field with x and z components:

$$\boldsymbol{B}_0 = B_x \boldsymbol{e}_x + B_z \boldsymbol{e}_z. \tag{A1}$$

The co-rotation velocity is expressed as

$$\boldsymbol{v}_0 = v_x \boldsymbol{e}_x + v_y \boldsymbol{e}_y, \tag{A2}$$

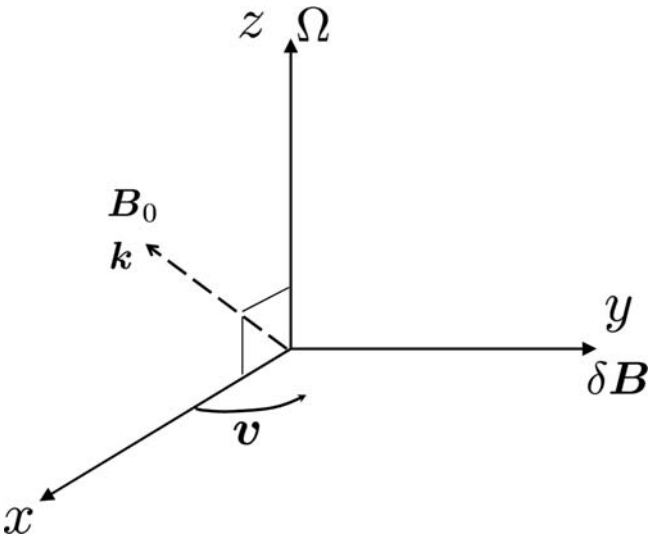

Figure A1. Geometry of the Alfvén wave propagating along the magnetic field line. The unperturbed fluid rotates around the spin axis, $\boldsymbol{v} = v_x \boldsymbol{e}_x + v_y \boldsymbol{e}_y$.

where $v_x = -\Omega y$ and $v_y = \Omega x$, respectively. We will assume a uniform perturbation of the magnetic field:

$$\delta \boldsymbol{B} \propto \delta B \boldsymbol{e}_y, \tag{A3}$$

where δB is constant in both $\boldsymbol{x}$ and time t. The linear differential equations for the equation of motion and the Maxwell equations are written as

$$\rho \left[\frac{\partial \delta \boldsymbol{v}}{\partial t} + (\boldsymbol{v}_0 \cdot \nabla)\delta \boldsymbol{v} + (\delta v \cdot \nabla)\boldsymbol{v}_0 \right] = \delta \boldsymbol{F}, \tag{A4}$$

$$\nabla \cdot \delta \boldsymbol{E} = 4\pi \delta \rho_{\rm e}, \tag{A5}$$

$$\nabla \cdot \delta \boldsymbol{B} = 0, \tag{A6}$$

$$\nabla \times \delta \boldsymbol{E} = -\frac{1}{c}\frac{\partial \delta \boldsymbol{B}}{\partial t} \tag{A7}$$

and

$$\nabla \times \delta \boldsymbol{B} = \frac{4\pi}{c}\delta \boldsymbol{j} + \frac{1}{c}\frac{\partial \delta \boldsymbol{E}}{\partial t}, \tag{A8}$$

where the perturbation of the Lorentz forces can be written down as

$$\delta \boldsymbol{F} = \delta \rho_{\rm e} \boldsymbol{E} + \rho_{\rm e} \delta \boldsymbol{E} + \frac{1}{c}(\delta \boldsymbol{j} \times \boldsymbol{B}_0 + \boldsymbol{j} \times \delta \boldsymbol{B}), \tag{A9}$$

where $\rho_{\rm e}$ and $\boldsymbol{j} = \rho_{\rm e} \boldsymbol{v}_0$ are background charge density and current, respectively. The background charge density, $\rho_{\rm e}$, is described by the Goldreich–Julian charge density, i.e. $\rho_{\rm e} = \nabla \cdot \boldsymbol{E}/4\pi = -\nabla \cdot (\boldsymbol{v}_0 \times \boldsymbol{B}_0)/4\pi \sim -\Omega B_z/2\pi c$. The remaining equation is given by the frozen in condition

$$\delta \boldsymbol{E} = -\frac{1}{c}(\delta \boldsymbol{v} \times \boldsymbol{B}_0 + \boldsymbol{v}_0 \times \delta \boldsymbol{B}). \tag{A10}$$

We may seek a solution in the form of the plane wave propagating along the background magnetic field:

$$\boldsymbol{f} \propto \exp\{{\rm i}[k(b_x x + b_z z) - \omega t]\}, \tag{A11}$$

where $b_x = B_x/B$, $b_z = B_z/B$, ω is the wave frequency and k is the magnitude of the wavenumber. As this take place in the set of the linear equations (A4)–(A9), we can obtain the electric field as

$$\delta E_x = -b_z(-\beta_\phi + b_x\beta_x)\delta B,\ \delta E_y = 0,$$
$$\delta E_z = -(b_x\beta_\phi + \beta_x b_z^2)\delta B, \tag{A12}$$

and the current as

$$\delta j_x = -\mathrm{i}\frac{kc}{4\pi}(b_z\delta B - \beta_\phi\delta E_x),\ \delta j_y = 0,$$
$$\delta j_z = \mathrm{i}\frac{kc}{4\pi}(b_x\delta B + \beta_\phi\delta E_z), \tag{A13}$$

where $\beta_\phi = \omega/kc$ is the phase velocity in units of the speed of light and $\beta_x = v_x/c$.

The dispersion relation is given by

$$(b_x\beta_x - \beta_\phi)^2 - \frac{b_x^2\Omega^2}{k^2c^2} + b_z^2\beta_x^2\beta_{\rm A}^2 - \beta_{\rm A}^2(1-\beta_\phi^2) = 0, \tag{A14}$$

where $\beta_{\rm A} = v_{\rm A}/c$ with $v_{\rm A} = B_0/\sqrt{4\pi\rho}$ being the Alfvén velocity. Usually, the second term in the left-hand side can be negligible because $\Omega/kc \sim \Omega/\omega \ll 1$. In the limit of $\beta_x \ll \beta_{\rm A}$ and $\beta_y = v_y/c \ll \beta_{\rm A}$, the phase velocity becomes

$$\beta_\phi^2 = \frac{\beta_{\rm A}^2}{1+\beta_{\rm A}^2}, \tag{A15}$$

which is the traditional dispersion relation for the Alfvén wave, and we obtain $\beta_\phi = 1$ for $\beta_{\rm A} \gg 1$ and $\beta_\phi = \beta_{\rm A}$ for $\beta_{\rm A} \ll 1$.

The electric field parallel ($\delta E_{||}$) and perpendicular ($\delta E_\perp$) to the background magnetic field can be described by

$$\delta E_{||} \equiv |\delta\boldsymbol{E}\cdot\boldsymbol{B}_0| = |b_z\beta_x\delta B| \tag{A16}$$

and

$$\delta E_\perp \equiv |\delta\boldsymbol{E}\times\boldsymbol{B}_0| = |\beta_\phi\delta B|, \tag{A17}$$

respectively. For the current, we obtain

$$\delta j_{||} = -\mathrm{i}\frac{\omega}{4\pi}b_z\beta_x\delta B \tag{A18}$$

and

$$\delta j_\perp = \mathrm{i}\frac{kc}{4\pi}(1-\beta_\phi^2)\delta B, \tag{A19}$$

respectively. The important result is that the electric field and current along the magnetic field are exited due to the rotation of the unperturbed matter, and hence the electrons and/or positrons can be accelerated along the magnetic field line.

In the limit of $\beta_{\rm A} \gg 1$ ($\beta_\phi = 1$), we find that

$$(\delta E_{||},\ \delta E_\perp) \sim -\delta B(b_z\beta_x,\ 1). \tag{A20}$$

Hence the magnitude of the induced electric field is in order of magnitude of the perturbed magnetic field. The current becomes

$$(\delta j_{||},\ \delta j_\perp) \sim \mathrm{i}\frac{\omega}{4\pi}\delta B(-b_z\beta_x,\ \beta_{\rm A}^{-2}), \tag{A21}$$

implying the parallel current dominates the perpendicular current.

In the limit of $\beta_{x,y} \ll \beta_{\rm A} \ll 1$ ($\beta_\phi = \beta_{\rm A}$), the electric field and the current become

$$(\delta E_{||},\ \delta E_\perp) \sim -\delta B(b_z\beta_x, \beta_\phi) \tag{A22}$$

and

$$(\delta j_{||},\ \delta j_\perp) \sim \mathrm{i}\frac{\omega}{4\pi}\delta B(-b_z\beta_x,\ \beta_{\rm A}^{-1}), \tag{A23}$$

respectively. The magnitude of induced electric field is much smaller than that of the perturbed magnetic field.

Finally, if $\beta_{\rm A} \sim \beta_{x,y} \ll 1$, we will see the phase velocity

$$\beta_\phi \sim b_x\beta_x \pm \beta_{\rm A}. \tag{A24}$$

This paper has been typeset from a TEX/LATEX file prepared by the author.